

Article

Influence of Co-Content on the Optical and Structural Properties of TiO_x Thin Films Prepared by Gas Impulse Magnetron Sputtering

Patrycja Pokora¹, Damian Wojcieszak^{1,*}, Piotr Mazur², Małgorzata Kalisz³ and Malwina Sikora^{1,4}

¹ Faculty of Electronics, Photonics and Microsystems, Wrocław University of Science and Technology, Janiszewskiego 11/17, 50-372 Wrocław, Poland

² Institute of Experimental Physics, University of Wrocław, Max Born 9, 50-204 Wrocław, Poland

³ Faculty of Engineering and Economics, Ignacy Mościcki State Vocational University in Ciechanów, Narutowicza 9, 06-400 Ciechanów, Poland

⁴ Nanores Company, Bierutowska 57–59, 51-317 Wrocław, Poland

* Correspondence: damian.wojcieszak@pwr.edu.pl; Tel.: +48-713202375

Abstract: Nonstoichiometric (Ti,Co)O_x coatings were prepared using gas-impulse magnetron sputtering (GIMS). The properties of coatings with 3 at.%, 19 at.%, 44 at.%, and 60 at.% Co content were compared to those of TiO_x and CoO_x films. Structural studies with the aid of GIXRD indicated the amorphous nature of (Ti,Co)O_x. The fine-columnar, homogeneous microstructure was observed on SEM images, where cracks were identified only for films with a high Co content. On the basis of XPS measurements, TiO₂, CoO, and Co₃O₄ forms were found on their surface. Optical studies showed that these films were semi-transparent ($T > 46\%$), and that the amount of cobalt in the film had a significant impact on the decrease in the transparency level. A shift in the absorption edge position (from 337 to 387 nm) and a decrease in their optical bandgap energy (from 3.02 eV to more than 2.60 eV) were observed. The hardness of the prepared films changed slightly (ca. 6.5 GPa), but only the CoO_x film showed a slightly lower hardness value than the rest of the coatings (4.8 GPa). The described studies allowed partial classification of non-stoichiometric (Ti,Co)O_x thin-film materials according to their functionality.

Keywords: oxide thin films; TiO_x; (Ti,Co)O_x; CoO_x; cobalt; gas impulse magnetron sputtering; semitransparent; amorphous coatings



Citation: Pokora, P.; Wojcieszak, D.; Mazur, P.; Kalisz, M.; Sikora, M. Influence of Co-Content on the Optical and Structural Properties of TiO_x Thin Films Prepared by Gas Impulse Magnetron Sputtering. *Coatings* **2023**, *13*, 955. <https://doi.org/10.3390/coatings13050955>

Academic Editor: Ana-Maria Lepadatu

Received: 31 March 2023

Revised: 12 May 2023

Accepted: 15 May 2023

Published: 19 May 2023



Copyright: © 2023 by the authors. Licensee MDPI, Basel, Switzerland. This article is an open access article distributed under the terms and conditions of the Creative Commons Attribution (CC BY) license (<https://creativecommons.org/licenses/by/4.0/>).

1. Introduction

Materials based on mixtures of Ti and Co oxides have recently gained attention because of their wide range of applications in electronics. Today, there are only a few reports on Co-doped TiO₂ [1–5], but mainly in the form of nanopowders, nanoparticles, or nanowires, while thin-film work itself is in a minority. One of the possible reasons for this fact is that the properties of such oxide mixtures are strongly related to the preparation method and additional postprocessing, such as high-temperature annealing. Therefore, a direct comparison of their properties is impossible. There exist only a few reports related to complex modification of the structural, surface, optical, or electrical properties of titanium dioxide as a matrix by doping with Co [6–9].

Our previous work is one of the few examples of such studies [10,11]. We have shown how interesting properties and applications can be obtained by combining the advantages of Ti and Co oxides. For example, the gradient coatings that we obtained were transparent and had a high refractive index despite the high content of cobalt [11]. More interesting is the fact that these coatings exhibited a fully recoverable resistive switching effect, which has not been previously reported in the case of such materials (Figure 1a). Their great potential can be used in innovative transparent electronic devices with a memory effect. Furthermore,

we also prepared transparent (~80%) oxide films based on titanium with a homogeneous distribution of cobalt [10]. In their case, a unipolar memristive effect was also observed, but only for coatings with a low cobalt content (Figure 1b). To date, no similar results have been reported. The aim of the present work was to manufacture nonstoichiometric (Ti,Co)O_x materials (with reduced oxygen content) in order to obtain a lower resistivity as compared to the mentioned coatings. A compromise between optical and electrical properties was planned to be achieved. In addition, we decided to prepare films with a higher amount of cobalt because of the small number of publications in this field.

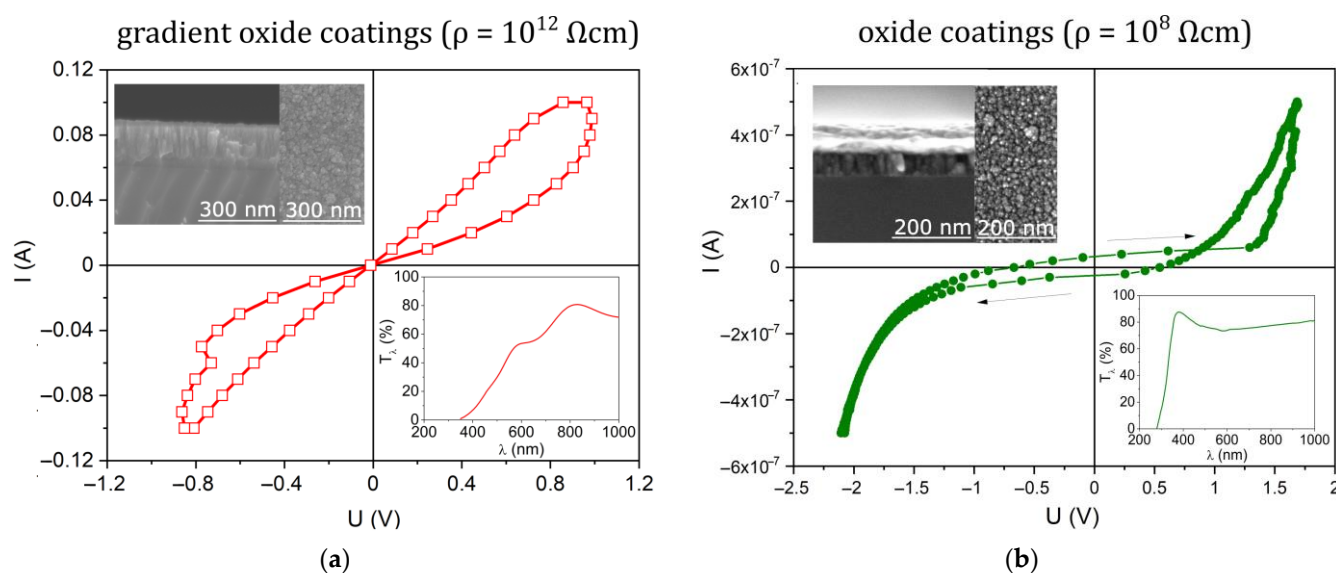


Figure 1. Current to voltage (I–V) of transparent (a) gradient [11] and (b) oxide [10] coatings (Ti,Co)O_x that exhibit a memristive effect. In the insets, SEM images of surface and cross-section, as well as transmission characteristics, are shown.

The influence of Co on the properties of Ti-based oxides is not yet well understood, which limits the possibility of fully exploiting the potential that the combination of these two materials can offer. Cobalt and its oxides exhibit high stability (especially in the form of CoO and Co₃O₄) [12], as well as high photocatalytic activity [13] and ferromagnetic properties [14]. Co-based oxides and metallic materials can be applied in spintronics [15], magneto-optical devices [16], in the construction of semiconducting sensors [17], electrochromic coatings [18], and heterogeneous catalysts [19]. The properties of oxides based on titanium and cobalt are significantly dependent on their preparation technology. These materials are mostly manufactured in the form of nanotubes [1], nanowires [2], nanorods [3], nanoparticles [4], or various types of thin-film coating (single films or multilayers) [5] (Figure 2). Nanotubes, nanowires, and nanorods make up the largest part of the (Ti,Co)O_x forms reported in publications (Figure 2). The hydrothermal [2] or anodisation [1,3] methods are used mainly for their manufacture. The form of nanotubes is interesting for electrochemical applications (e.g., fuel cells) due to their ability to transport electrons unidirectionally and their large surface area [20,21]. These types of nanomaterials exhibit improved catalytic properties [22,23]. In the case of nanowires, an application in efficient photoelectrochemical (PEC) hydrolysis can be presented [2]. Nanorods, on the other hand, are useful in the oxygen evolution reaction (OER), which is a key process in many technologies, including the conversion of electrochemical energy or the production of zinc–air batteries [3]. Unlike the mentioned forms, these oxides are often manufactured as nanoparticles [4,6,9], which are useful in energy storage or solar energy conversion [4].

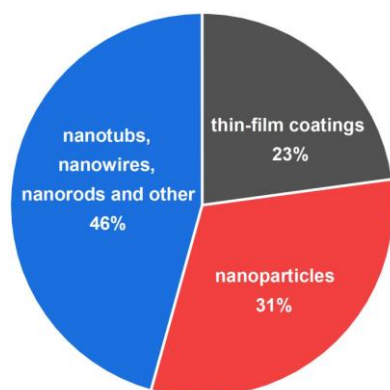


Figure 2. Percentage number of publications on various Ti- and Co-based oxide materials ($\text{TiO}_2\text{:Co}$, $\text{TiO}_2+\text{CoO}_x$, $\text{Ti}_x\text{Co}_{x-1}\text{O}_y$) [based on the ScienceDirect database from 1980 to 2022].

Nanoparticles are usually manufactured by sol-gel [9], hydrothermal [8], calcination [24], pyrolysis [25], or plasma thermal treatment [26] methods (Figure 3a). It should be noted that in the case of nanoparticles, typically only crystalline titanium dioxide is identified, and the influence of Co content on their properties has not been well explored [4,26]. Crystallite sizes depend not only on the amount of cobalt but are also determined by the preparation method of given nanoparticles. Therefore, it is difficult to define the relationship between Co content and crystallite size [4,6,8,9,26,27]. Oxide material-based Ti and Co are also prepared as thin-film coatings. They can have the form of single films [5,10,28,29] and multilayers [30–32] (Figure 3b). According to the literature, magnetron sputtering [10,33–35], Metal Organic Chemical Vapor Deposition (MOCVD) [28], epitaxy [5], or sol-gel [7,36] are primarily used for their manufacture. Their (material composition (Co-content) can also vary significantly [29,34,37]. Modification of the sputtering conditions results in the receipt of diversified thin-film materials, which is important in their application area [2,33]. As mentioned above, in the case of oxide nanomaterials based on titanium and cobalt, their material composition is a key factor.

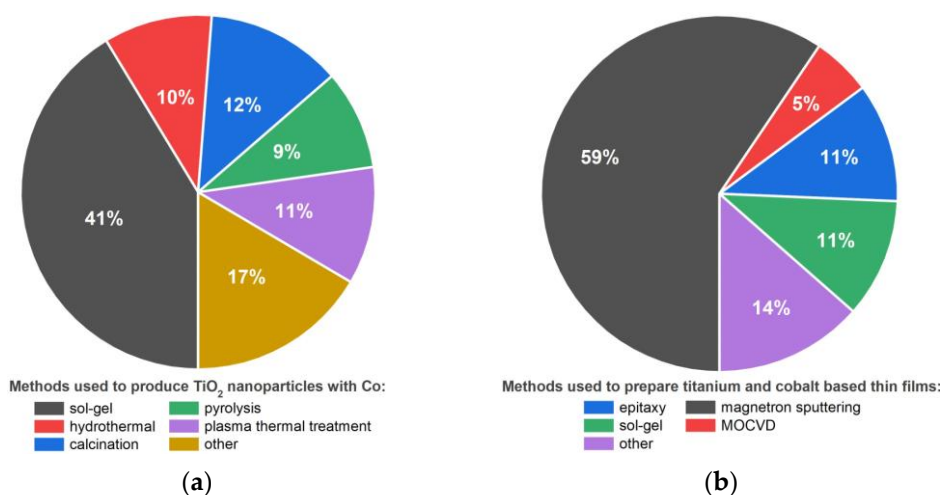


Figure 3. Methods used to prepare TiO_2 nanoparticles doped with Co (a); preparation methods of thin films based on Ti and Co mixed oxides (b) based on the ScienceDirect database from 1980 to 2022.

The current state of the art indicates that in nanoparticles, as well as in thin-film coatings, the amount of cobalt is usually below 15 at.% [5,27,38] (Figure 4), although there are some reports that present results for materials with even 50 at.% or 76 at.% cobalt [26,29]. As can be seen, there is a research gap regarding materials with cobalt content comparable to or greater than titanium. As an analysis of the literature shows, most of these materials are crystalline [5,25,38], while approximately 14% of the total work has been devoted to

amorphous materials [31,39]. Therefore, it can be seen that the main focus has been on investigating the influence of cobalt on TiO_2 properties only within a narrow range of this element, completely discounting what modifications in $(\text{Ti,Co})\text{Ox}$ films would be introduced by a higher amount of cobalt. This fact itself makes conducting research for $(\text{Ti,Co})\text{Ox}$ coatings with a higher content of cobalt a novelty in the field of the materials in discussion.

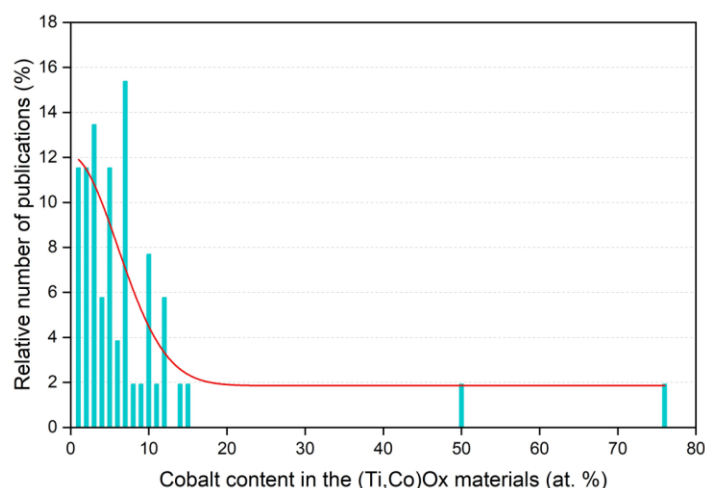


Figure 4. Relative number of publications describing cobalt content in $(\text{Ti,Co})\text{Ox}$ films based on the ScienceDirect database from 1980 to 2022.

Among crystalline materials, $(\text{Ti,Co})\text{Ox}$ can generally be distinguished by nanoparticles [6,9,37] or also by thin films (but mainly annealed) [28,37,40]. In the case of nanoparticles (often prepared with the sol–gel method), TiO_2 with anatase or rutile structure is dominant, while the presence of cobalt as separate phases (oxide or metallic) or as a compound with titanium or its oxides [8] occurs rarely with nanoparticles. However, there exist some works in which crystal forms of their compounds (e.g., CoTiO_2 or Co_2TiO_2) have been identified [26]. Accurate studies on titanium- and cobalt-based thin films are rare, especially in non-stoichiometric (i.e., low oxygen amount) forms. In addition, there is a general strong need to develop multifunctional coatings [10]. This paper investigates the influence of the amount of cobalt on the optical and structural properties of non-stoichiometric thin films based on titanium and cobalt.

2. Materials and Methods

2.1. Preparation of Thin Films

Nonstoichiometric $(\text{Ti,Co})\text{Ox}$ thin films with the desired material composition were prepared using the gas impulse magnetron sputtering method (denoted as GIMS). Magnetrons were supplied by an MSS2 2 kW pulsed AC power supply unit (DORA Power System, Wilczyce, Poland) [41–46]. The sputtering system was also equipped with vacuum gauges (Pfeiffer Vacuum, Aßlar, Germany) and a gas flow control system that involves mass flow controllers (MKS Instruments, Andover, MA, USA). In the applied GIMS processes, a gas mixture ($\text{Ar}:\text{O}_2$) with a low O_2 content (10:1) was injected into the working chamber directly on the surface of the metallic Ti, Co, and Ti-Co targets (diameter-30 mm, thickness 3 mm, purity 99.95%) mounted on the magnetron. Ti-Co targets with 2 at.%, 12 at.%, and 50 at.% Co content were used for preparation. Targets were prepared with spark plasma sintering (SPS) using a system provided by FCT GmbH (Rauenstein, Germany) [47–49]. For sintering, Co and Ti nanopowders (99.95%, Kurt Lesker, Dresden, Germany) in the Lukasiwicz Research Network–Institute of Non-Ferrous Metals [49] were used. The targets were sintered at 1200 °C in a graphite matrix. The material composition of the targets was determined using a JXA-8230 X-ray microanalyzer (JEOL) with wave and energy-dispersive spectrometers (WDS and EDS). A detailed description of the Ti-Co target

preparation method was described elsewhere [10]. Due to the possibility of sputtering in multimagnetron configuration (Ti,Co)O_x thin films with various Co content (3, 19, 44, and 60 at.%) were obtained. In addition, TiO_x and CoO_x reference films were prepared. The Ar:O₂ gas mixture was obtained due to the use of a gas mixer that includes two individual MKS mass flow controllers. Ar and O₂ flow rates were set at 30 and 3 sccm, respectively. Gas impulses, injected directly into the target, were synchronised with the magnetron supply unit (MSS2 type, Dora Power System), and in each cycle lasted 100 ms. The locally ignited plasma was obtained at $<6 \times 10^{-3}$ mbar, with a supply power of 500 W (500 V, 1 A). The plasma ignition time was 30 ms and the interval between pulses was 70 ms. The sputtering system was equipped with diffusion and rotary pumps. Before the GIMS processes, the vacuum chamber was evacuated to a base pressure of ca. 5×10^{-6} mbar. Thin films were deposited on Si and SiO₂ substrates. The distance between the target and the substrate was 16 cm. Figure 5 shows a schematic layout of thin film preparation.

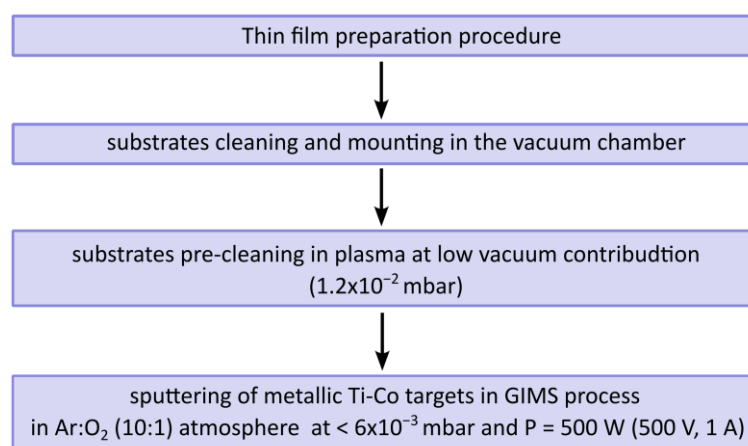


Figure 5. Schematic layout of (Ti,Co)O_x thin-film preparation.

2.2. Methods of Thin Film Characterisation

The surface morphology of the coatings and their chemical composition were investigated using a high-quality SEM/Xe-FIBFEI Helios NanoLab 600i field-emission scanning electron microscope (FEI, Hillsboro, OR, USA) equipped with an energy dispersive X-ray spectrometer (EDS). In addition, high-resolution SEM images of the surface and cross-sections were examined. Analysis of Ti and Co concentrations on the basis of EDS maps of the elemental distribution was also carried out. The structural properties of the thin films were determined based on the results of GIXRD in the incidence mode of grazing (at 3°) mode. For the measurements, an Empyrean X-ray diffractometer (PANalytical, Malvern, UK) with a PIXel3D detector and Cu K α radiation with a wavelength of 1.5406 Å (40 kV, 30 mA) using Bragg-Brentano reflecting geometry parafocusing optics was used. By comparing the obtained pattern with PDFcards, a phase structure was determined. For data analysis, MDI JADE 5.0 software (ICDD, Newtown Square, PA, USA) was used. For the analysis of the surface state, X-ray photoelectron spectroscopy (XPS) was used. The Specs Phoibos 100 MCD-5 (5 single-channel electron multiplier) hemispherical analyser (SPECS Surface Nanoanalysis GmbH, Berlin, Germany) using a Specs XR-50 X-ray source with Mg K α (1253.6 eV) beam was used. The XPS spectra were analysed using Casa XPS software. The thicknesses of the manufactured films were verified with the aid of a contactless Taylor Hobson Tally Surf CCI Lite optical profiler (Talysurf CCI Lite, Leicester, UK). The nanoindentation technique was used to determine the hardness of the prepared thin films. The hardness was obtained from experimental load–displacement curves for an indentation experiment using the Oliver and Pharr method [50,51]. Measurements were made with a CSM Instruments (CSM Instruments, Peseux, Switzerland) NHTT 01-03620 nanoindenter model equipped with a Vickers diamond indenter. For optical characterisation, the light transmission method was used. The measurement setup was equipped with an integrated

light source DH-2000-BAL (containing a halogen and deuterium lamp) and Ocean Optics QE 65000 and NIR 256-2.1 spectrophotometers (Ocean Optics, Largo, FL, USA). The transmission coefficient was determined from transmittance spectra measured in the wavelength range of 250–2000 nm. The average transmission was evaluated by calculating the integral in visible wavelength range of 300 to 900 nm. On the basis of the measurements, parameters such as the light transmission coefficient (T_λ), position of the optical absorption edge ($\lambda_{\text{cut-off}}$), and the width of the optical band gap (E_g^{opt}) were determined.

3. Results and Discussion

3.1. Material Composition of (Ti,Co)Ox Thin Films

In Figure 6b, SEM images of surface topography with EDS maps of elemental distribution of (Ti,Co)Ox thin films are shown. It was found that films with 3 at.%, 19 at.%, 44 at.%, 60 at.%, and 100 at.% of cobalt content in the TiO_x matrix were prepared. EDS maps indicate a homogeneous distribution of Ti, O, and Co, as well as a lack of agglomeration effects. The absence of areas with a clearly higher concentration of cobalt should be emphasised because it proves the high quality of sintered targets and the possibility of manufacturing Ti-based oxide coatings with a homogeneous distribution of Co. Detailed results of the EDS analysis are collected in Table 1.

Table 1. Material composition of thin-film coatings based on Ti and Co and targets used for their deposition by magnetron sputtering.

Target	Co-Content in the Film (at.%)
Ti	-
Ti _{0.98} Co _{0.02}	3
Ti _{0.88} Co _{0.12}	19
Ti _{0.88} Co _{0.12} + Ti _{0.50} Co _{0.50}	44
Ti _{0.50} Co _{0.50}	60
Co	100

3.2. Optical Characterisation of (Ti,Co)Ox Thin Films

The optical properties of the coatings were determined on the basis of transmission characteristics (Figure 7a). In the case of undoped TiO_x, the average transmission level of value $T_{\lambda_a} = 48\%$ (average transmission related to the area under the characteristic) was the highest compared to other films (Figure 7b). The addition of Co resulted in a decrease in the transparency. The (Ti,Co)Ox films with 3 at.% and 19 at.% of cobalt were semitransparent due to the 46% and 29% values of T_{λ_a} , respectively (Figure 7b). The increase in Co content resulted in a significant decrease in the transparency level to <10% for (Ti_{0.56}Co_{0.44})Ox and (Ti_{0.40}Co_{0.60})Ox, respectively. In the case of CoO_x, an opaque film was received ($T_{\lambda_a} < 2\%$) (Figure 7b). Except for analysis of transmission level, the position of the optical absorption edge ($\lambda_{\text{cut-off}}$) was determined (Figure 7a). It was found that with the increase of cobalt content, the $\lambda_{\text{cut-off}}$ position shifts to longer wavelengths ('red shift'). This effect has also been reported in other works [9,27], but it should be noted that the position of the optical absorption edge is also related to the preparation method. Therefore, the 'blue shift' of the $\lambda_{\text{cut-off}}$ can also be observed in oxide materials based on Ti and Co [7]. These results are in agreement with other works, e.g., [5,7,36,52–55]. In general, the transmission level of Ti oxides decreases with increasing Co content, but the preparation method and the form of (Ti,Co)Ox material (thin film or nanoparticles) determine these changes [52–54], as can be seen for the thin films, where the light transmission level decreases with increasing Co content [7,36,52].

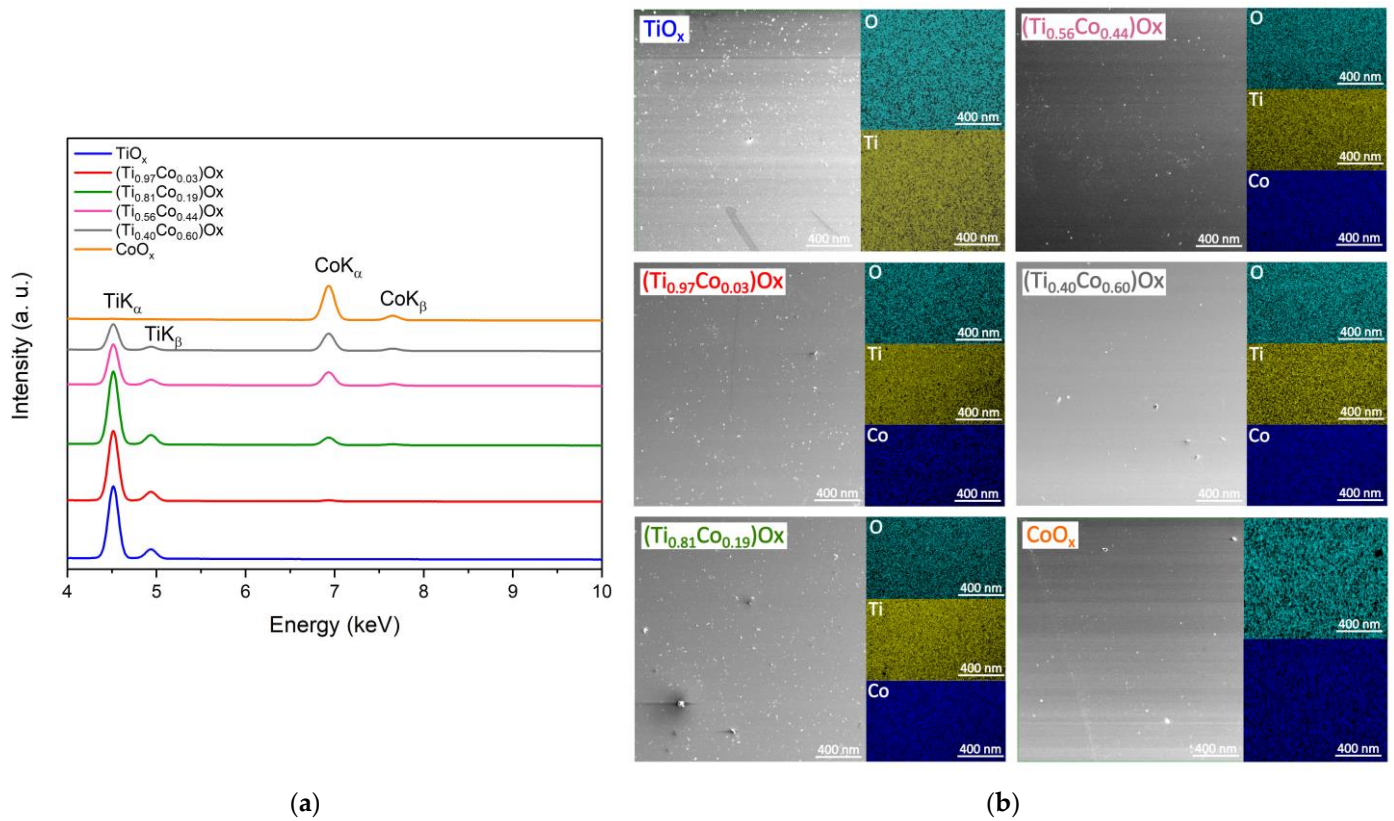


Figure 6. Results of X-ray microanalysis investigations for as-deposited Ti, Co, and O for (Ti,Co)Ox thin films: (a) EDS spectra and (b) maps of elemental distribution of mixed oxides.

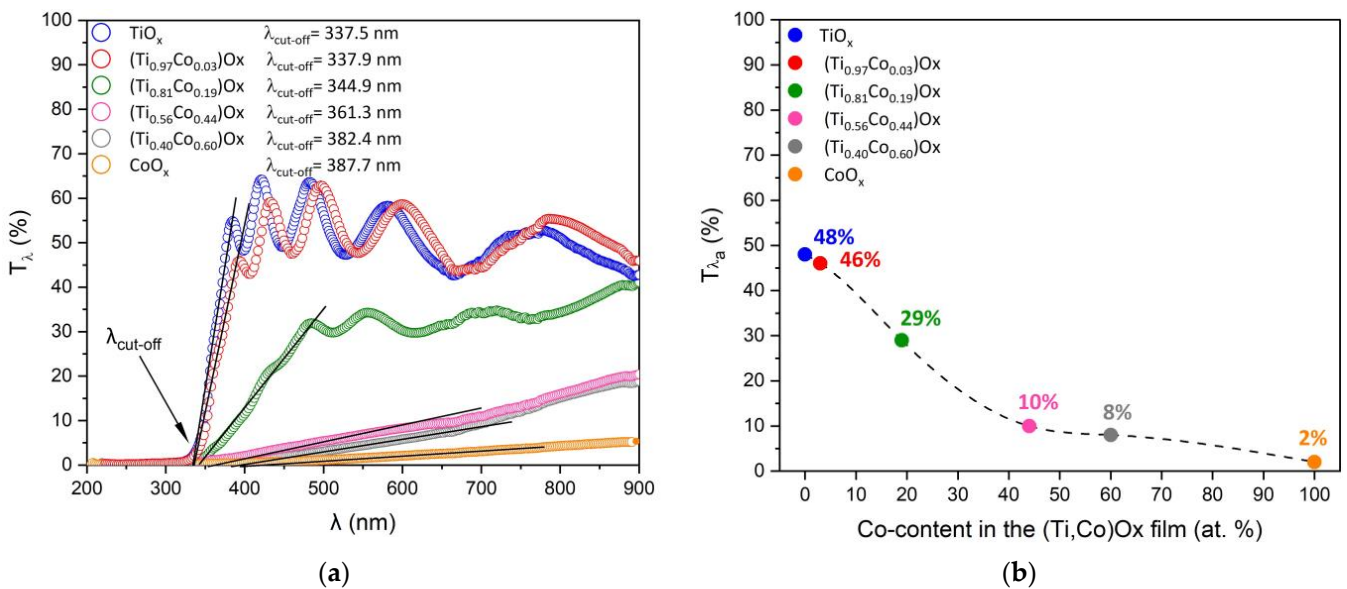


Figure 7. Transmission characteristics of TiO_x ($t = 410$ nm), (Ti_{0.97}Co_{0.03})O_x ($t = 335$ nm), (Ti_{0.81}Co_{0.19})O_x ($t = 480$ nm), (Ti_{0.56}Co_{0.44})O_x ($t = 270$ nm), (Ti_{0.40}Co_{0.60})O_x ($t = 226$ nm), and CoO_x ($t = 150$ nm) thin films (a) with average transmission level (T_{λ_a}) as a function of the cobalt content in the film (b). Designations: T_{λ} —transmission, T_{λ_a} —average transmission in the range of 300 to 900 nm, t —thickness of the films.

Films containing a low amount of cobalt are characterised by a level of transparency similar to that of undoped TiO_2 or the mentioned nanoparticles (ca. 80%). Above 10 at.% cobalt results in a significant reduction of transmission (Figure 8a). However, the literature lacks comprehensive analyses of titanium oxide coatings with neither low nor high Co content. A significantly different character can be seen for nanoparticles (Figure 8b) [9,21,25,27]. These nanomaterials have a similar value of the light transmission coefficient (from 60% to 90%). It is difficult to determine the reason for the lack of changes with the increase in Co content. This can be determined by the manufacturing method or may be related to the fact that the core of the nanoparticles is TiO_2 and cobalt is located in its shell [9,25,27]. The solution to this shortcoming may be additional annealing, which will almost certainly cause oxygenation of the film structure.

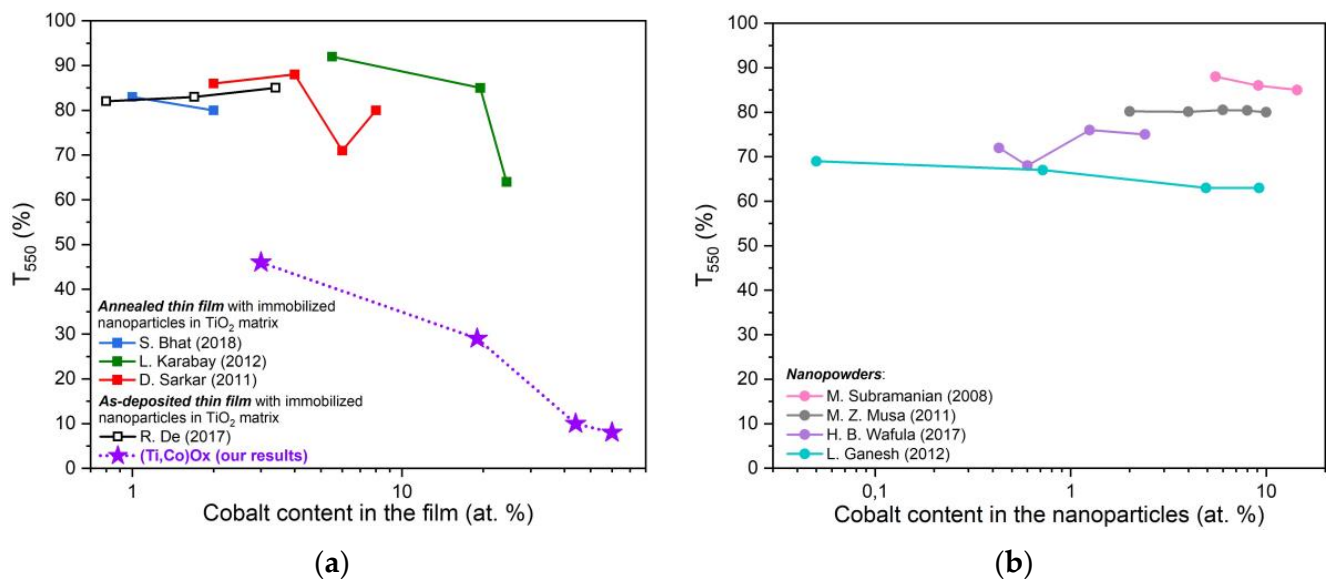


Figure 8. Influence of cobalt content on the optical energy gap coefficient of oxide materials based on Ti: (a) thin films with immobilised nanoparticles in the TiO_x matrix [7,52–54]; (b) nanopowders [9,21,25,27]. On the basis of data from the publication, the cobalt content was converted from wt.% to at.%.

Based on transmission characteristics, the Tauc plots (for indirect transitions) were obtained and the optical band gap was estimated (Figure 9). The E_g^{opt} values for the TiO_x and $(\text{Ti}_{0.97}\text{Co}_{0.03})\text{O}_x$ films were very similar and equal to 3.08 and 3.02 eV, respectively. The increase in the Co content resulted in a decrease in the E_g^{opt} value. In the case of the film with 19 at.% of Co, 2.26 eV was noticed. For films with greater amounts of cobalt, a transmission level that was too low did not allow us to determine the value of the optical band gap. However, it should be noted that the results obtained are consistent with reports in the literature [6,56]. The results available for thin films show the crucial role of their form and method of preparation. There is a general tendency for the value of E_g to decrease with the increase of Co content [7,21,25,27,52–54,57] (Figure 10).

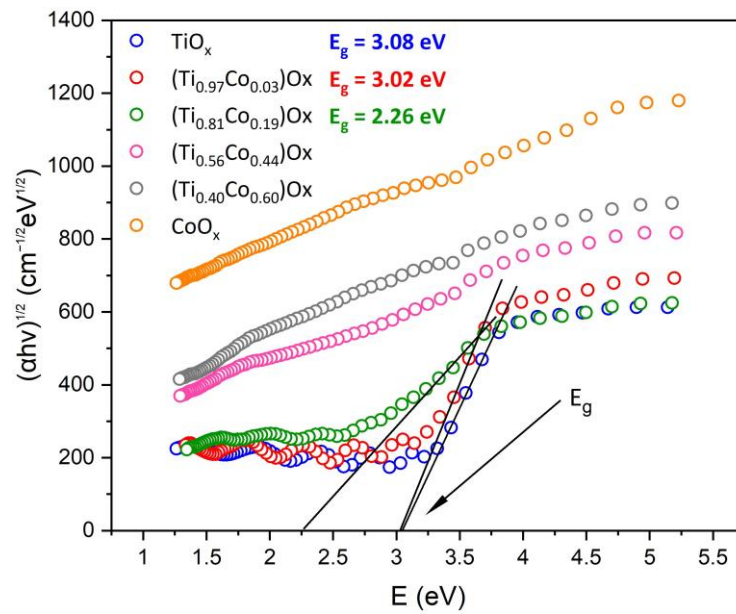


Figure 9. Tauc plots for the thin films of TiO_x , $(\text{Ti,Co})\text{O}_x$, and CoO_x with marked areas of determination of the optical band gap (E_g^{opt}).

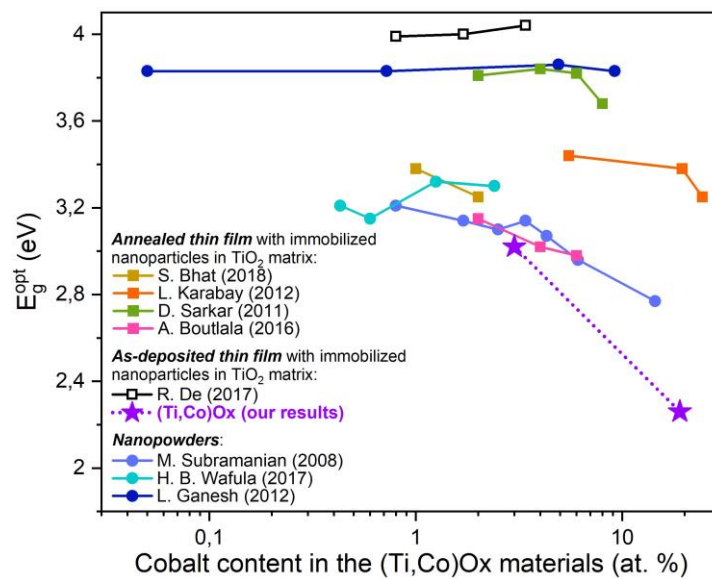


Figure 10. Influence of cobalt content on the light transmission coefficient of oxide materials based on Ti [7,21,25,27,52–54,57]. On the basis of data from the publication, the cobalt content was converted from wt.% to at.%.

3.3. Structural Characterisation of Thin Films of $(\text{Ti,Co})\text{O}_x$

In Figure 11, SEM images of the surface and cross-sectional topography of the prepared oxide films are shown. It can be stated that the microstructure of all coatings from the GIMS processes was very homogeneous.

Cross-sectional images indicate that the TiO_x and $(\text{Ti,Co})\text{O}_x$ films had a columnar character. Their microstructure was densely packed and free of cracks or gaps between columns. The increase in Co content resulted in a decrease in the width of the columns from 30 to 15 nm. The lack of titanium in the film resulted in a microstructure of a different nature, i.e., grainy. This means that the presence of titanium has a key influence on the process of nucleation of $(\text{Ti,Co})\text{O}_x$ coatings in the GIMS process.

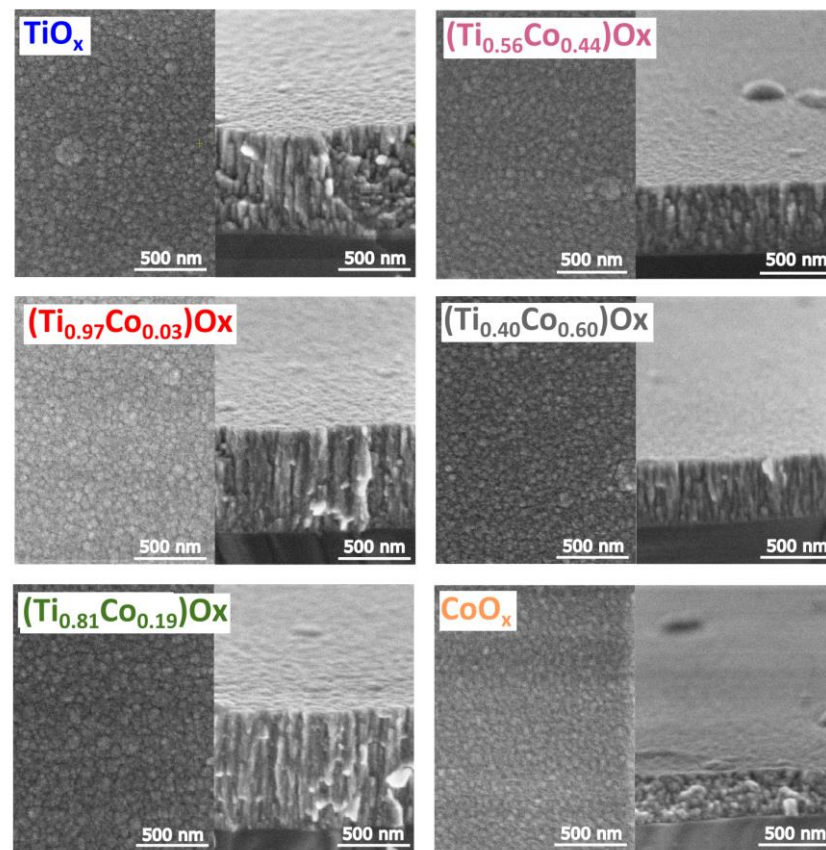


Figure 11. SEM images of the surface and cross-sectional topography of TiO_x , $(\text{Ti,Co})\text{O}_x$, and CoO_x thin films.

The structure of the as-deposited $(\text{Ti,Co})\text{O}_x$ coatings was examined using X-ray diffraction (XRD) in the grazing incidence mode (GIXRD). In Figure 12, the GIXRD patterns of the films are shown.

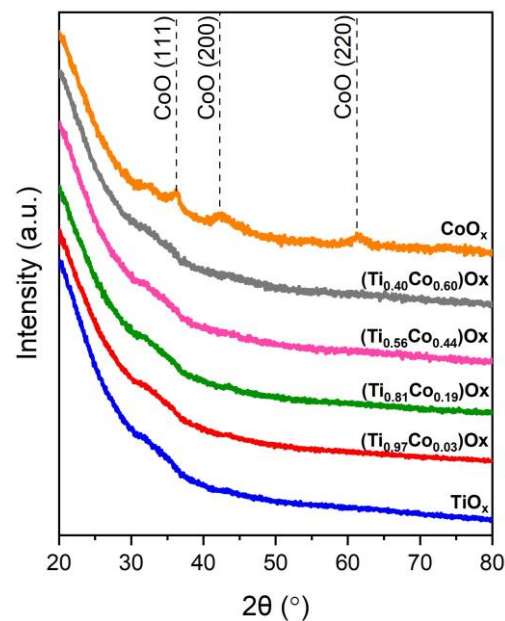


Figure 12. GIXRD patterns of TiO_x , $(\text{Ti,Co})\text{O}_x$, and CoO_x thin films prepared by gas impulse magnetron sputtering.

As can be seen, all coatings prepared by the GIMS technique were amorphous except for CoO_x , which was nanocrystalline. In this case, the crystalline form of CoO was identified, but it should be emphasised that the intensity of the peaks in the pattern is very weak.

Furthermore, broad peaks were also exposed in patterns related to the SiO_2 substrate. However, there is a lack of peaks that could testify about the crystal form of titanium, cobalt, or their oxides. Similar results were also obtained for other oxide materials prepared using the GIMS technique [44–46], which is a consequence of this innovative sputtering method [42]. Detailed results of the XRD analysis are collected in Table 2.

Table 2. Structural properties of TiO_x , $(\text{Ti},\text{Co})\text{O}_x$, and CoO_x thin films, based on GIXRD measurements.

Thin Film	Phase (-)	(hkl) (-)	D (nm)	d (nm)	d_{PDF} (nm)	a^1 (Å)
CoO_x	CoO	(111)	4.1	0.24597	0.24807	4.26033
	CoO	(200)	4.0	0.21302	0.21687	4.33740
	CoO	(220)	4.1	0.15062	0.15125	4.26018
$(\text{Ti}_{0.40}\text{Co}_{0.60})\text{O}_x$						
$(\text{Ti}_{0.56}\text{Co}_{0.44})\text{O}_x$						
$(\text{Ti}_{0.81}\text{Co}_{0.19})\text{O}_x$						
$(\text{Ti}_{0.97}\text{Co}_{0.03})\text{O}_x$						
TiO_x						

D—average crystallite size; d—interplanar distance; d_{PDF} —standard interplanar distance, a—lattice parameters; ¹ Similar results were obtained in publications [58–60].

The influence of the Co content on the hardness of nonstoichiometric Ti-based films with the aid of nanoindentation was also investigated. Figure 13 shows the results of hardness as a function of the relative indenter displacement for all prepared TiO_x , $(\text{Ti},\text{Co})\text{O}_x$, and CoO_x coatings. There was no significant change in the hardness value (H) with increasing cobalt. The value of H was in the range of 6.3 GPa to 6.9 GPa. Only for the CoO_x film was a lower value (4.8 GPa) observed (Figure 14). These results may testify to the influence of the type of microstructure on the hardness. Thus, the TiO_x and $(\text{Ti},\text{Co})\text{O}_x$ films with columnar microstructure had a similar hardness, whereas the grainy microstructure of the CoO_x film resulted in ca. 25% lower hardness. However, there is a lack of data related to the hardness of such mixed Ti-Co oxide materials, especially non-stoichiometric.

Because the GIXRD results did not reveal the forms in which cobalt of titanium occurred in the $(\text{Ti},\text{Co})\text{O}_x$ coatings, we decided to perform photoelectron spectroscopy (XPS). In Figure 15, the XPS survey spectra recorded for composite bonding are shown [61–64].

In Figure 16 the XPS spectra recorded for Ti2p peaks recorded for $(\text{Ti},\text{Co})\text{O}_x$ and TiO_x thin films are shown. For all films, the presence of a characteristic doublet of Ti2p peaks can be observed. The positions of both $\text{Ti}2p_{3/2}$ and $\text{Ti}2p_{1/2}$ photoelectron peaks correspond to the +4 oxidation state of titanium [61,62,65,66]. The differences in the positions of the Ti2p doublet peaks are very small, i.e., below 0.1 eV (Figure 17). Therefore, the amount of Co addition does not affect the position of the Ti2p doublet. This suggests that titanium only forms its distinct oxide forms and not compounds with cobalt. It should also be noted that the difference in the position of the peaks in the doublet (ΔBE) itself, which is in the range of 5.6 to 5.7 eV, indicates the presence of the TiO_2 form (Figure 17).

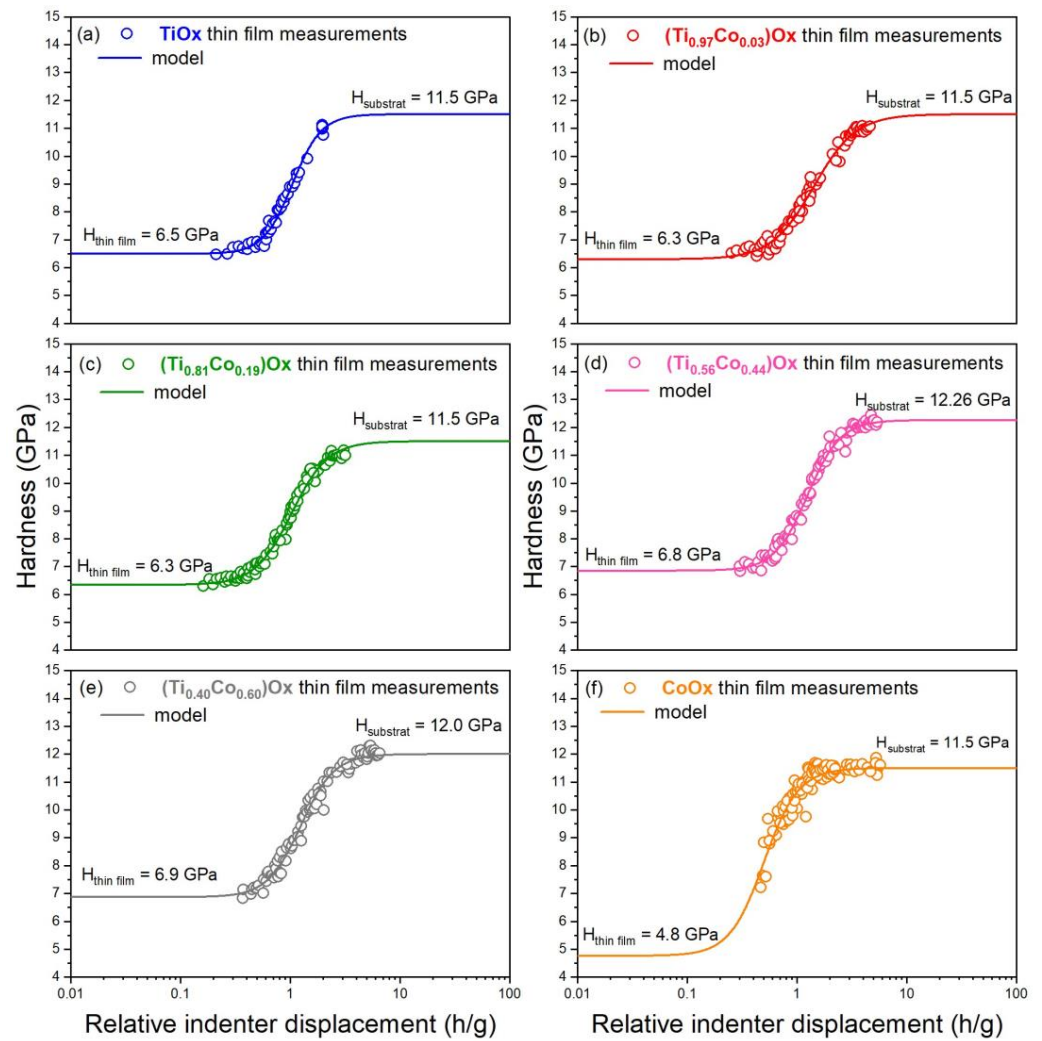


Figure 13. Hardness of (a) TiO_x , (b) $(\text{Ti}_{0.93}\text{Co}_{0.03})\text{O}_x$, (c) $(\text{Ti}_{0.81}\text{Co}_{0.19})\text{O}_x$, (d) $(\text{Ti}_{0.56}\text{Co}_{0.44})\text{O}_x$, (e) $(\text{Ti}_{0.40}\text{Co}_{0.60})\text{O}_x$ and (f) CoO_x oxide thin films.

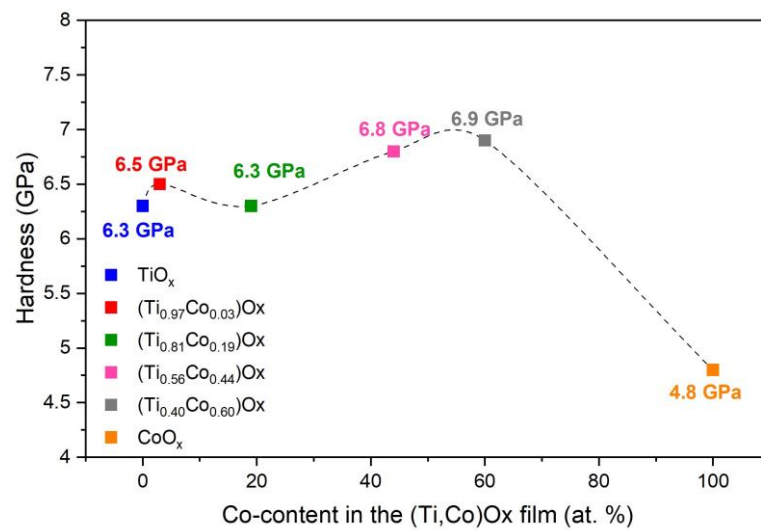


Figure 14. The effect of cobalt on the hardness of TiO_x films.

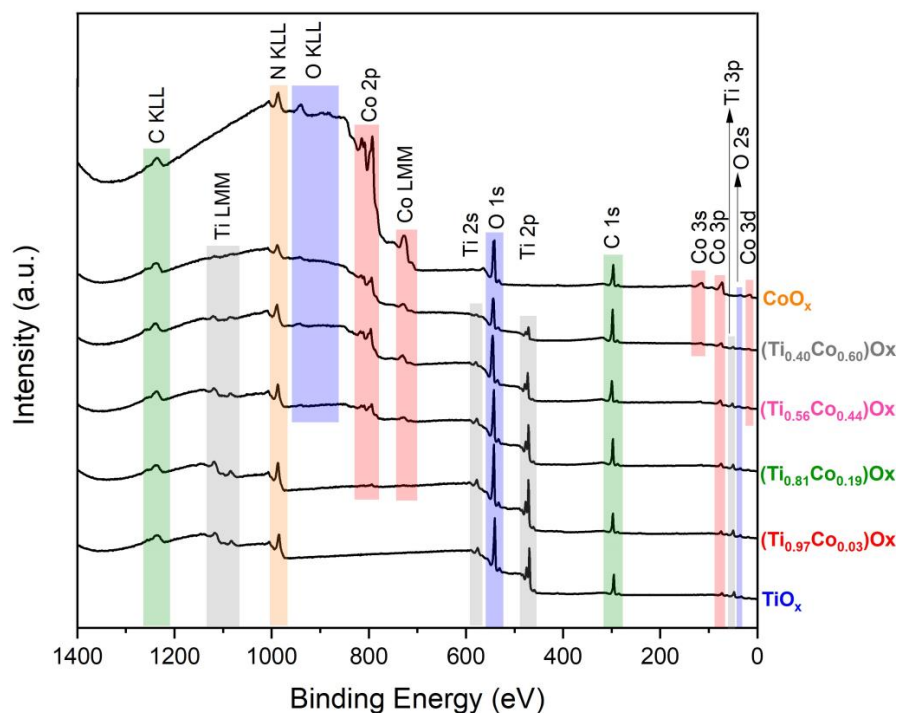


Figure 15. XPS survey spectra of the as-deposited TiO_x , $(\text{Ti,Co})\text{O}_x$, and CoO_x thin films.

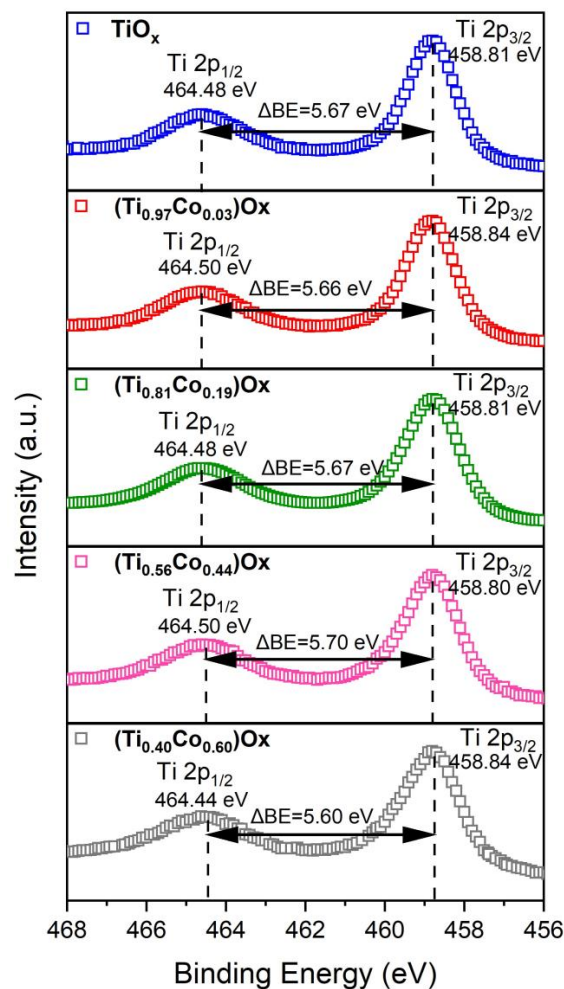


Figure 16. The XPS spectra of the $\text{Ti}2p$ state for TiO_x and $(\text{Ti,Co})\text{O}_x$ thin films.

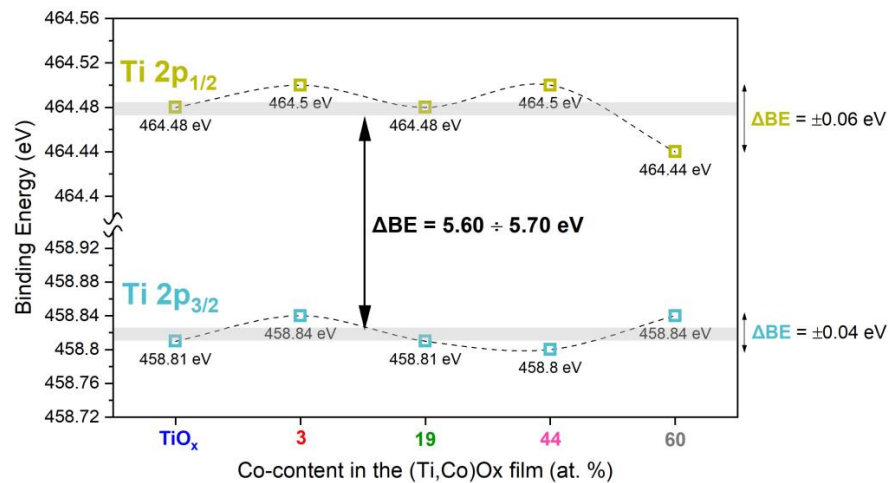


Figure 17. The influence of Co content on the position of Ti2p doublet peak.

Figure 18 presents the XPS spectra for the O1s peaks recorded for the prepared TiO_x , $(\text{Ti,Co})\text{O}_x$, and CoO_x thin films. Deconvolution of the multipeak (Figure 19a) showed that it consisted of three peaks, centred on: (i) 530.3 eV, attributed to lattice oxygen [61,62,66,67]; (ii) 532.1 eV, related to the presence of hydroxyl groups (OH^-) on the surface [61,62,66,67]; and (iii) 533.6 eV, related to the water molecules adsorbed on the surface ($\text{H}_2\text{O}_{\text{ads}}$) [61,62,66]. The differences in the positions of the O1s doublet peaks are very small, i.e., below 0.5 eV. Taking into account the intensity of the multipeak O1s (Figure 19b), it could be concluded that the surfaces of $(\text{Ti,Co})\text{O}_x$ with 44 at.% and 60 at.% cobalt, as well as CoO_x thin films, are more likely to absorb OH^- from the surrounding environment than TiO_x and $(\text{Ti,Co})\text{O}_x$ with 19 at.% or 3 at.% Co. Furthermore, with increasing Co content, the level of $\text{H}_2\text{O}_{\text{ads}}$ also increased from 2% to 15%.

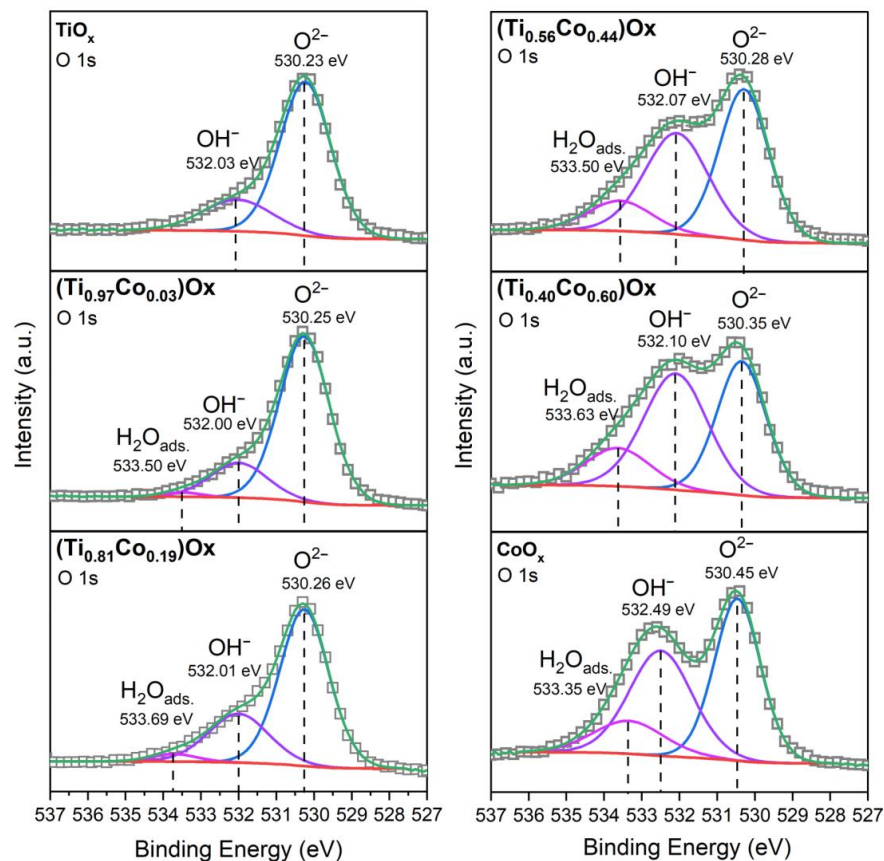
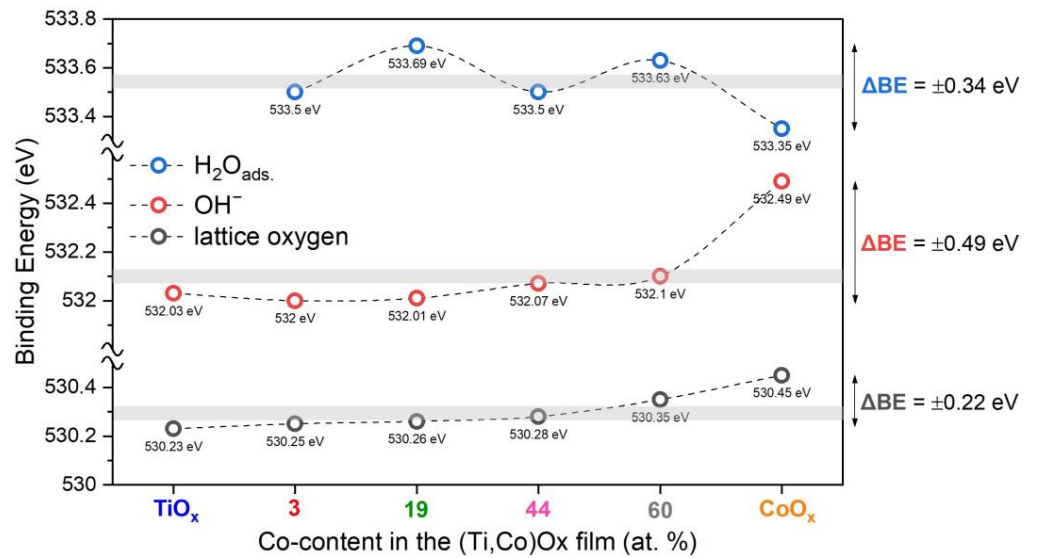
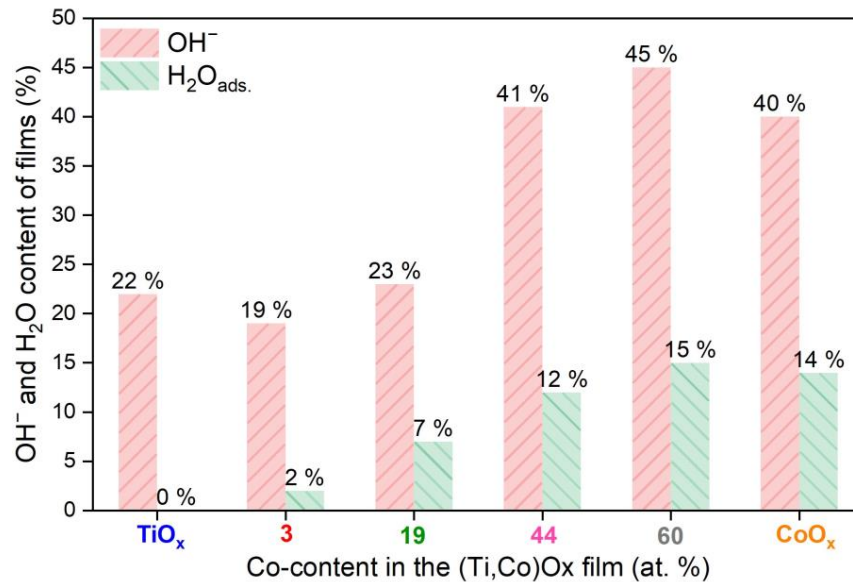


Figure 18. XPS spectra for the O1 state of TiO_x , $(\text{Ti,Co})\text{O}_x$, and CoO_x thin films.



(a)



(b)

Figure 19. The influence of cobalt content on the position of O1 multiplex (a); the relative content of OH groups and H₂O_{ads.} molecules adsorbed on the surface of prepared coatings to the O1 signal (b).

The most important part of the XPS research was the analysis of the spectra recorded for the Co2p state. We aimed to reveal the degree of oxidation of cobalt ions and thus the forms in which its oxides may occur in the coatings. In Figure 8a, the Co2p_{3/2} spectra of prepared (Ti,Co)O_x and CoO_x thin films are shown. In each spectrum, a multiplex can be observed (Figure 20). It was deconvoluted into a satellite (786.5 eV) and two main peaks.

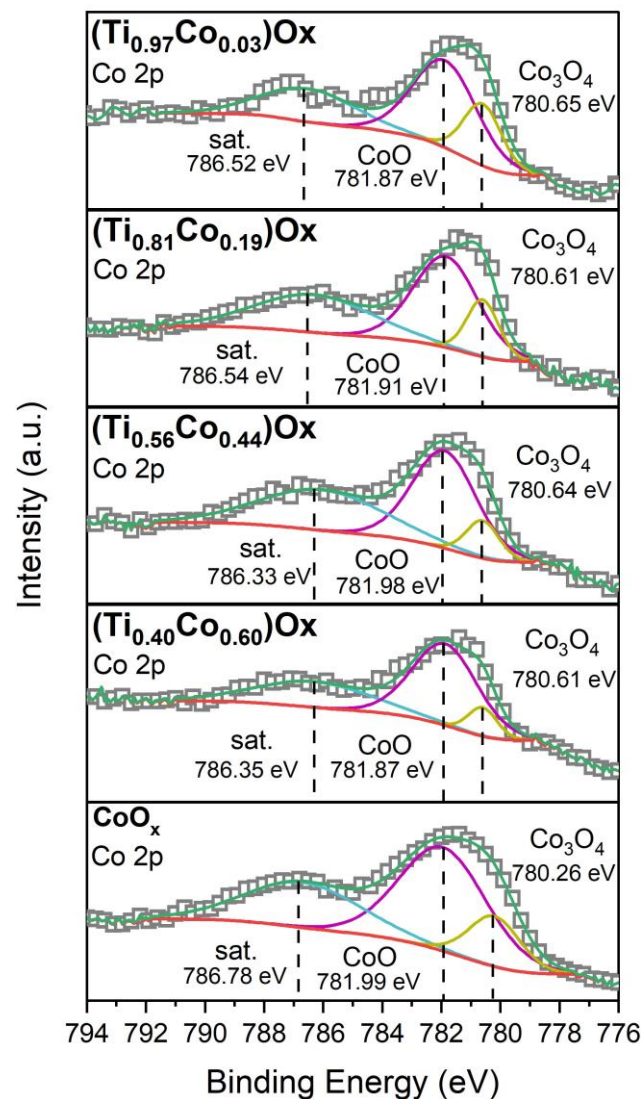


Figure 20. XPS spectra for $\text{Co}2p_{3/2}$ state of $(\text{Ti},\text{Co})\text{O}_x$ and CoO_x thin films.

The first $\text{Co}2p_{3/2}$ peak centred at approximately 781.8 eV is related to Co^{2+} ions; thus, the presence of the CoO form can be confirmed [61,62,68–70]. The second $\text{Co}2p_{3/2}$ peak of $\text{Co}2p_{3/2}$ located at approximately 780.6 eV corresponds to Co^{2+} and Co^{3+} ions and can be related to the appearance of Co_3O_4 [61,62,68–71]. However, some authors argue that, based on XPS measurements of Co_2O_3 and Co_3O_4 , which contain both Co^{2+} and Co^{3+} , cannot be distinguished by chemical shift or satellite [21]. This suggests that the surface films of Co_2O_3 and Co_3O_4 are similar. The binding energy values estimated for $\text{Co}2p_{3/2}$ core levels are in agreement with those reported for Co oxides in the literature [61,62,68–70]. There are no references to mixed oxides in the literature, while quite a few examples involve single oxides. Due to the very low number of literature reports on such materials, it was relatively difficult to compare the peaks to $\text{Co}2p_{3/2}$ spectra. Comparison of the areas under the peaks revealed that the percentage of Co ions in the +2 oxidation state is about 3–4 times that of +3. Differences in the positions of the $\text{Co}2p_{3/2}$ doublet peaks are very small, i.e., below 0.5 eV (Figure 21a). Furthermore, with an increase in the Co content in the $(\text{Ti},\text{Co})\text{O}_x$ films, the percentage content of the CoO form increases at the expense of Co_3O_4 (Figure 21b).

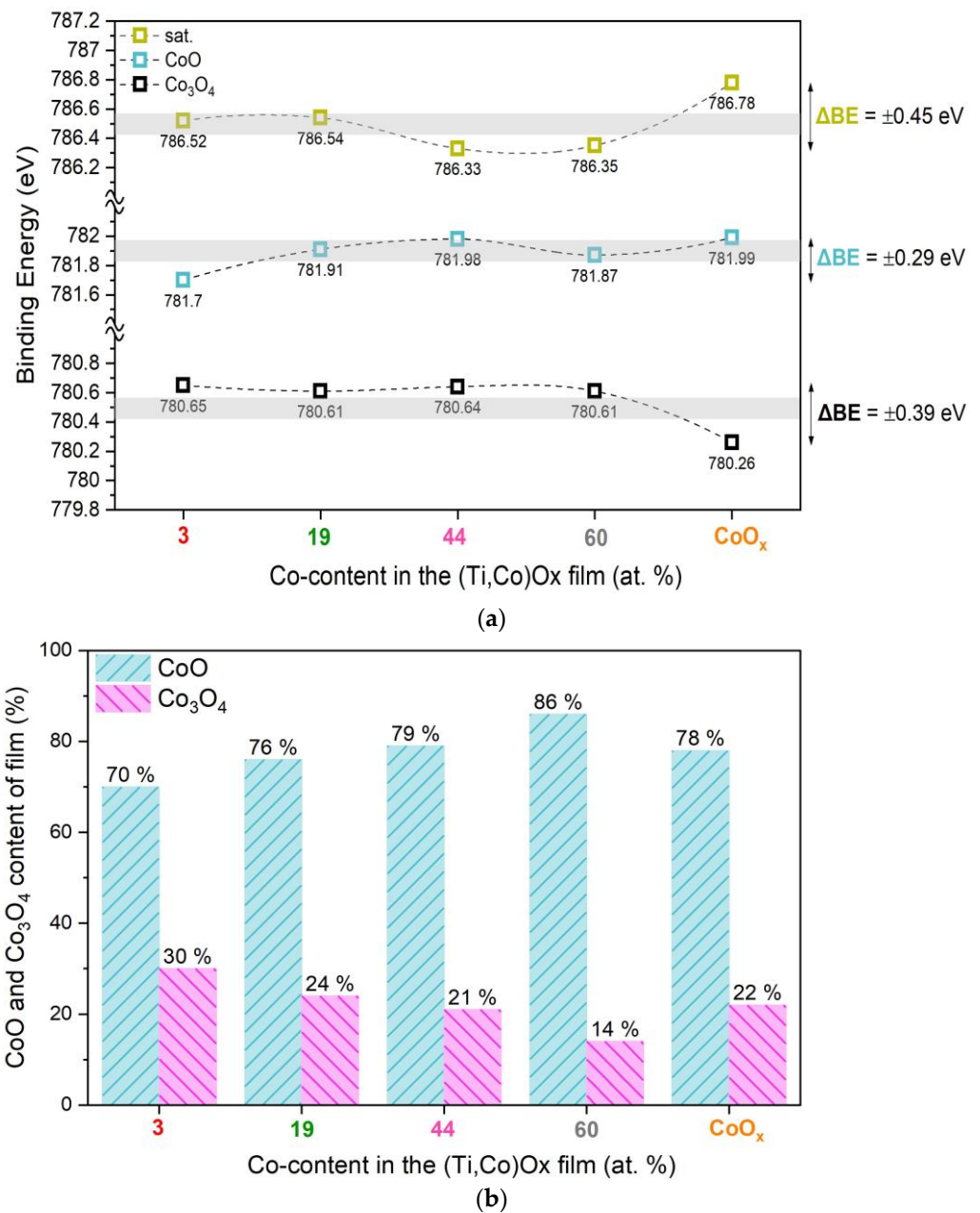


Figure 21. The influence of cobalt on the multippeak position of Co2p_{3/2} (a); the content of adsorbed hydroxy groups and water molecules on the surface of the examined coatings (b).

4. Conclusions

In this work, the influence of the Co content on the properties of non-stoichiometric (Ti,Co)O_x thin films prepared by a GIMS process has been described. The aim of our research was to obtain a broad change in the material composition for coatings prepared under the same conditions. The application of gas impulse sputtering resulted in the manufacture of amorphous (Ti,Co)O_x films with a homogeneous distribution of cobalt. The change in Co content resulted in modification of the morphology and optical properties. The most significant changes were observed for the optical parameters. A large drop in the transparency level and the optical band gap was observed along with the increase in the cutoff wavelength ('red shift'). Structural studies revealed that, except for the nanocrystalline CoO_x film (with crystallites of <5 nm in size) with fine-grained microstructure, the morphology of all amorphous TiO_x and (Ti,Co)O_x coatings had a columnar nature. The hardness of TiO_x and (Ti,Co)O_x films (6.5 GPa) was higher compared to CoO_x (4.8 GPa).

The XPS analysis has revealed that the prepared films consisted of mixed oxides. For all (Ti,Co)Ox films, the occurrence of TiO₂ form was observed, while in the cobalt, the additive was present in its own forms. The occurrence of CoO and Co₃O₄ forms was identified. The quantity of cobalt ions in the +2 state was 3–4 times higher compared to the +3 ions. However, modification of the composition of the material resulted in a decrease in CoO at the expense of Co₃O₄ with an increase in the cobalt content of the film.

Author Contributions: Conceptualization, P.P. and D.W.; methodology, P.P. and D.W.; validation, D.W.; investigation, P.P., M.S., M.K., P.M. and D.W.; resources, D.W.; writing—original draft preparation, P.P. and D.W.; writing—review and editing, P.P. and D.W.; supervision, D.W. All authors have read and agreed to the published version of the manuscript.

Funding: This work was co-financed from the sources given by the Polish National Science Centre (NCN) as a research project number 2018/29/B/ST8/00548.

Institutional Review Board Statement: Not applicable.

Informed Consent Statement: Not applicable.

Data Availability Statement: Not applicable.

Conflicts of Interest: The authors declare no conflict of interest.

Abbreviations

The following table shows all abbreviations used in this work.

a	lattice parameters
d	interplane distance
d _{PDF}	standard interplane distance (according to PDF card)
D	average crystallite size
E	energy
E _g	width of the energy gap
E _g ^{opt.}	width of the optical energy gap
H _{substrate}	hardness of the substrate
H _{thin film}	hardness of the thin film
h	Planck's constant
T _λ	light transmission coefficient
T ₅₅₀	average value of the light transmission coefficient for the wavelength λ = 550 nm
T _{λa}	average transmission in the range of 300 to 900 nm
t	thickness of the films
α	absorption coefficient
λ	wavelength of electromagnetic radiation
λ _{cut-off}	position of the edge of optical absorption
EDS	energy-dispersive spectroscopy
(Ti _{0.97} Co _{0.03})Ox	abbreviated notation of the thin film as a mixture of oxides in which the atomic content is: 97% at. Ti to 3% at. Co
PDF	powder diffraction files
SEM	transmission electron microscopy
XPS	X-ray photoelectron spectroscopy
XRD	grazing incidence X-ray diffraction

References

1. Venturini, J.; Bonatto, F.; Guaglianoni, W.C.; Lemes, T.; Arcaro, S.; Alves, A.K.; Bergmann, C.P. Cobalt-doped titanium oxide nanotubes grown via one-step anodization for water splitting applications. *Appl. Surf. Sci.* **2019**, *464*, 351–359. [[CrossRef](#)]
2. Liu, C.; Wang, F.; Zhu, S.; Xu, Y.; Liang, Q.; Chen, Z. Controlled charge-dynamics in cobalt-doped TiO₂ nanowire photoanodes for enhanced photoelectrochemical water splitting. *J. Colloid Interface Sci.* **2018**, *530*, 403–411. [[CrossRef](#)] [[PubMed](#)]
3. Yang, C.; Makabu, C.M.; Du, X.; Li, J.; Sun, D.; Liu, G. Cobalt nanorods decorated titanium oxide arrays as efficient and stable electrocatalyst for oxygen evolution reaction. *Electrochim. Acta* **2021**, *396*, 139213. [[CrossRef](#)]
4. Khan, W.; Ahmad, S.; Hassan, M.M.; Naqvi, A.H. Structural phase analysis, band gap tuning and fluorescence properties of Co doped TiO₂ nanoparticles. *Opt. Mater.* **2014**, *38*, 278–285. [[CrossRef](#)]

5. Yamada, Y.; Toyosaki, H.; Tsukazaki, A.; Fukumura, T. Epitaxial growth and physical properties of a room temper ferromagnetic semiconductor: Anatase phase $Ti_{1-x}Co_xO_2$. *J. Appl. Phys.* **2004**, *96*, 5097. [[CrossRef](#)]
6. Husain, S.; Alkhtaby, L.A.; Giorgetti, E.; Zoppi, A.; Miranda, M.M. Influence of cobalt doping on the structural, optical and luminescence properties of sol-gel derived TiO_2 nanoparticles. *Philos. Mag.* **2017**, *97*, 17–27. [[CrossRef](#)]
7. Bhat, S.; Sandeep, K.M.; Kumar, P.; Dharmaprasanth, S.M.; Byrappa, K. Characterization of transparent semiconducting cobalt doped titanium dioxide thin films prepared by sol–gel process. *J. Mater. Sci. Mater. Electron.* **2018**, *29*, 1098–1110. [[CrossRef](#)]
8. Jiang, P.; Xiang, W.; Kuang, J.; Liu, W.; Cao, W. Effect of cobalt doping on the electronic, optical and photocatalytic properties of TiO_2 . *Solid State Sci.* **2015**, *46*, 27–32. [[CrossRef](#)]
9. Musa, M.Z.; Ameran, Z.F.; Mamat, M.H.; Malek, M.F.; Rasheid, B.A.; Noor, U.M.; Rusop, M. Effects of cobalt doping concentration on the structural, electrical, and optical properties of titanium dioxide thin films. In Proceedings of the 2011 International Conference on Electronic Devices, Systems and Applications (ICEDSA), Kuala Lumpur, Malaysia, 25–27 April 2011; pp. 339–342. [[CrossRef](#)]
10. Wojcieszak, D.; Mazur, M.; Pokora, P.; Wrona, A.; Bilewska, K.; Kijaszek, W.; Kotwica, T.; Posadowski, W.; Domaradzki, J. Properties of metallic and oxide thin films based on Ti and Co prepared by magnetron sputtering from sintered targets with different Co-content. *Materials* **2021**, *14*, 3797. [[CrossRef](#)]
11. Wojcieszak, D.; Domaradzki, J.; Pokora, P.; Sikora, M.; Mazur, M.; Chodasewicz, P.; Morgiel, J.; Gibson, D. Optical and structural properties of gradient $(Ti,Co)O_x$ thin-film coatings with a resistive switching effect. *Appl. Opt.* **2022**, *34*, 10283–10289. [[CrossRef](#)]
12. Mei, J.; Liao, T.; Ayoko, G.A.; Bell, J.; Sun, Z. Cobalt oxide-based nanoarchitectures for electrochemical energy applications. *Prog. Mater. Sci.* **2019**, *103*, 596–677. [[CrossRef](#)]
13. Verma, M.; Mitan, M.; Kim, H.; Vaya, D. Efficient photocatalytic degradation of malachite green dye using facilely synthesized cobalt oxide nanomaterials using citric acid and oleic acid. *J. Phys. Chem. Solids* **2021**, *155*, 110125. [[CrossRef](#)]
14. Gajbhiye, N.S.; Sharma, S.; Nigam, A.K.; Ningthoujam, R.S. Tuning of single to multi-domain behavior for monodispersed ferromagnetic cobalt nanoparticles. *Chem. Phys. Lett.* **2008**, *466*, 181–185. [[CrossRef](#)]
15. Kaloyeros, A.E.; Pan, Y.; Goff, J.; Arles, B. Cobalt thin films: Trends in processing technologies and emerging applications. *ECS J. Solid State Sci. Technol.* **2019**, *8*, 119–152. [[CrossRef](#)]
16. Hirohata, A.; Yamada, K.; Nakatani, Y.; Prejbeanu, I.L.; Dieny, B.; Pirro, P.; Hillebrands, B. Review on spintronics: Principles and device applications. *J. Magn. Magn. Mater.* **2020**, *509*, 166711. [[CrossRef](#)]
17. Bewan, S.; Ndolomingo, M.J.; Meijboom, R.; Bingwa, N. Cobalt oxide promoted tin oxide catalysts for highly selective glycerol acetalization reaction. *Inorg. Chem. Commun.* **2021**, *128*, 108578. [[CrossRef](#)]
18. Svegl, F.; Orel, B.; Hutchins, M.G.; Kalcher, K. Structural and Spectroelectrochemical Investigations of sol-gel derived electrochromic spinel Co_3O_4 films. *J. Electrochem. Soc.* **1996**, *143*, 1532. [[CrossRef](#)]
19. Bahlawane, N.; Rivera, E.F.; Hoinghaus, K.K.; Brechling, A.; Kleineberg, U. Characterization and tests of planar Co_3O_4 model catalysts prepared by chemical vapor deposition. *Appl. Catal. B Environ.* **2004**, *53*, 245–255. [[CrossRef](#)]
20. Yao, W.; Fang, H.; Ou, E.; Wang, J.; Yan, Z. Highly efficient catalytic oxidation of cyclohexane over cobalt-doped mesoporous titania with anatase crystalline structure. *Catal. Commun.* **2006**, *7*, 387–390. [[CrossRef](#)]
21. Ganesh, I.; Gupta, A.K.; Kumar, P.P.; Sekhar, P.S.C.; Radha, K.; Padmanabham, G.; Sundararajan, G. Preparation and characterization of Co-doped TiO_2 materials for solar light induced current and photocatalytic applications. *Mater. Chem. Phys.* **2012**, *135*, 220–234. [[CrossRef](#)]
22. Wang, H.; Wang, J.; Wu, Z.; Liu, Y. NO catalytic oxidation behaviors over CoO_x/TiO_2 catalysts synthesized by sol–gel method. *Catal. Lett.* **2010**, *134*, 295–302. [[CrossRef](#)]
23. Yang, W.H.; Kim, M.H.; Ham, S.W. Effect of calcination temperature on the low-temperature oxidation of CO over CoO_x/TiO_2 catalysts. *Catal. Today* **2007**, *123*, 94–103. [[CrossRef](#)]
24. Sadanandam, G.; Lalitha, K.; Kumari, V.D.; Shankar, M.V.; Subrahmanyam, M. Cobalt doped TiO_2 : A stable and efficient photocatalyst for continuous hydrogen production from glycerol: Water mixtures under solar light irradiation. *Int. J. Hydrogen Energy* **2013**, *38*, 9655–9664. [[CrossRef](#)]
25. Wafula, H.B.; Musembi, R.J.; Juma, A.; Tonui, P.; Simiyu, J.; Sakwa, T.; Prakash, D.; Verma, K.D. Compositional analysis and optical properties of Co doped TiO_2 thin films fabricated by spray pyrolysis method for dielectric and photocatalytic applications. *Optik* **2017**, *128*, 212–217. [[CrossRef](#)]
26. Li, J.G.; Buchel, R.; Isobe, M.; Mori, T.; Ishigaki, T. Cobalt-doped TiO_2 nanocrystallites: Radio-frequency thermal plasma processing, phase structure, and magnetic properties. *J. Phys. Chem. C* **2009**, *113*, 8009–8015. [[CrossRef](#)]
27. Subramanian, M.; Vijayalakshmi, S.; Venkataraj, S.; Jayavel, R. Effect of cobalt doping on the structural and optical properties of TiO_2 films prepared by sol-gel process. *Thin Solid Films* **2008**, *516*, 3776–3782. [[CrossRef](#)]
28. Seong, N.J.; Yoon, S.G. Effects of Co-doping level on the microstructural and ferromagnetic properties of liquid-delivery metalorganic-chemical-vapor-deposited $Ti_{1-x}Co_xO_2$ thin films. *Appl. Phys. Lett.* **2002**, *81*, 4209. [[CrossRef](#)]
29. Song, H.Q.; Mei, L.M.; Zhang, Y.P.; Yan, S.S.; Ma, X.; Wang, Y.; Zhang, Z.; Chen, L.Y. Magneto-optical Kerr rotation in amorphous TiO_2/Co magnetic semiconductor thin films. *Phys. B Condens. Matter* **2007**, *388*, 130–133. [[CrossRef](#)]
30. Logacheva, V.A.; Lukin, A.N.; Afonin, N.N.; Serbin, O.V. Synthesis and optical properties of cobalt-modified titanium oxide films. *Opt. Spectrosc.* **2019**, *126*, 674–680. [[CrossRef](#)]

31. Ko, Y.; Park, D.S.; Seo, B.S.; Yang, H.J.; Shin, H.J.; Kim, J.Y.; Lee, J.H.; Lee, W.H.; Reucroft, P.J.; Lee, J.G. Studies of cobalt thin films deposited by sputtering and MOCVD. *Mater. Chem. Phys.* **2003**, *80*, 560–564. [[CrossRef](#)]
32. Quiroz, H.P.; Calderon, J.A.; Dussan, A. Magnetic switching control in Co/TiO₂ bilayer and TiO₂:Co thin films for magnetic-resistive random access memories (M-RRAM). *J. Alloys Compd.* **2020**, *840*, 155674. [[CrossRef](#)]
33. Quiroz, H.; Galindez, E.F.; Dussan, A. Ferromagnetic-like behavior of Co doped TiO₂ flexible thin films fabricated via co-sputtering for spintronic applications. *Heliyon* **2020**, *6*, e03338. [[CrossRef](#)]
34. Afonin, N.N.; Logacheva, V.A. Cobalt modification of thin rutile films magnetron-sputtered in vacuum. *Tech. Phys.* **2018**, *63*, 605–611. [[CrossRef](#)]
35. Griffin, K.A.; Pakhomov, A.B. Cobalt-doped anatase TiO₂: A room temperature dilute magnetic dielectric material. *J. Appl. Phys.* **2005**, *97*, 10D320. [[CrossRef](#)]
36. Ahmad, M.K.; Rasheid, N.A.; Ahmed, A.Z.; Abdullah, S.; Rusop, M. Study of cobalt doping on the electrical and optical properties of titanium dioxide thin film prepared by sol-gel method. In Proceedings of the 2008 IEEE International Conference on Semiconductor Electronics, Johor Bahru, Malaysia, 25–27 November 2008; pp. 561–565. [[CrossRef](#)]
37. Park, W.; Ortega-Hertogs, R.J.; Moodera, J.S. Semiconducting and ferromagnetic behavior of sputtered Co-doped TiO₂ thin films above room temperature. *J. Appl. Phys.* **2002**, *91*, 8093. [[CrossRef](#)]
38. Tian, J.; Deng, H.; Sun, L.; Kong, H.; Yang, P.; Chu, J. Effects of Co doping on structure and optical properties of TiO₂ thin films prepared by sol-gel method. *Thin Solid Films* **2012**, *520*, 5179–5183. [[CrossRef](#)]
39. Quiroz, H.P.; Dussan, A. Synthesis temperature dependence on magnetic properties of cobalt doped TiO₂ thin films for spintronic applications. *Appl. Surf. Sci.* **2019**, *484*, 688–691. [[CrossRef](#)]
40. Park, Y.R.; Kim, K.J. Structural and optical properties of rutile and anatase TiO₂ thin films: Effects of Co doping. *Thin Solid Films* **2005**, *484*, 34–38. [[CrossRef](#)]
41. Chodun, R.; Dypa, M.; Wicher, B.; Langier, K.N.; Okrasa, S.; Minikayev, R.; Zdunek, K. The sputtering of titanium magnetron target with increased temperature in reactive atmosphere by gas injection magnetron sputtering technique. *Appl. Surf. Sci.* **2022**, *574*, 151597. [[CrossRef](#)]
42. Zdunek, K.; Nowakowska-Langier, K.; Dora, J.; Chodun, R. Gas injection as a tool for plasma process control during coating deposition. *Surf. Coat. Technol.* **2013**, *228*, S367–S373. [[CrossRef](#)]
43. Skowronski, L.; Zdunek, K.; Nowakowska-Langier, K.; Chodun, R.; Trzcinski, M.; Kobierski, M.; Kustra, M.; Wachowiak, A.; Wachowiak, W.; Hiller, T.; et al. Characterization of microstructural, mechanical and optical properties of TiO₂ layers deposited by GIMS and PMS methods. *Surf. Coat. Technol.* **2015**, *282*, 16–23. [[CrossRef](#)]
44. Wiatrowski, A.; Mazur, M.; Obstarczyk, A.; Wojcieszak, D.; Kaczmarek, D.; Morgiel, J.; Gibson, D. Comparison of the physico-chemical properties of TiO₂ thin films obtained by magnetron sputtering with continuous and pulsed gas flow. *Coatings* **2018**, *8*, 412. [[CrossRef](#)]
45. Mazur, M. Analysis of the properties of functional titanium dioxide thin films deposited by pulsed DC magnetron sputtering with various O₂: Ar ratios. *Opt. Mater.* **2017**, *69*, 96–104. [[CrossRef](#)]
46. Mazur, M.; Wojcieszak, D.; Wiatrowski, A.; Kaczmarek, D.; Lubanska, A.; Domaradzki, J.; Mazur, P.; Kalisz, M. Analysis of amorphous tungsten oxide thin films deposited by magnetron sputtering for application in transparent electronics. *Appl. Surf. Sci.* **2021**, *570*, 151151. [[CrossRef](#)]
47. Lei, C.; Du, Y.; Zhu, M.; Huo, W.; Wu, H.; Zhang, Y. Microstructure and mechanical properties of in situ TiC/Ti composites with a laminated structure synthesized by spark plasma sintering. *Mater. Sci. Eng. A* **2021**, *812*, 141136. [[CrossRef](#)]
48. Wimler, D.; Lindemann, J.; Gammer, C.; Spoerk-Erdely, P.; Stark, A.; Clemens, H.; Mayer, S. Novel intermetallic-reinforced near- α Ti alloys manufactured by spark plasma sintering. *Mater. Sci. Eng. A* **2020**, *792*, 139798. [[CrossRef](#)]
49. Lis, M.; Wrona, A.; Mazur, J.; Dupont, C.; Kamińska, M.; Kopyto, D.; Kwarciński, M. Fabrication And Properties Of Silver Based Multiwall Carbon Nanotube Composite Prepared By Spark Plasma Sintering Method. *Arch. Metall. Mater.* **2015**, *60*, 1351–1355. [[CrossRef](#)]
50. Oliver, W.; Pharr, G. An improved technique for determining hardness and elastic modulus using load and displacement sensing indentation experiments. *J. Mater. Res.* **1992**, *7*, 1564–1583. [[CrossRef](#)]
51. Jung, Y.-G.; Lawn, B.; Martyniuk, M.; Huang, H.; Hu, X. Evaluation of elastic modulus and hardness of thin films by nanoindentation. *J. Mater. Res.* **2004**, *19*, 3076–3080. [[CrossRef](#)]
52. Karabay, I.; Yuksel, S.A.; Ongul, F.; Ozturk, S.; Asli, M. Structural and optical characterization of TiO₂ thin films prepared by sol-gel process. *Acta Phys. Pol. A* **2012**, *121*, 265–267. [[CrossRef](#)]
53. Sarkar, D.; Ghosh, C.K.; Maiti, U.N.; Chattopadhyay, K.K. Effect of spin polarization on the optical properties of Co-doped TiO₂ thin films. *Phys. B* **2011**, *406*, 1429–1435. [[CrossRef](#)]
54. De, R.; Tripathi, S.; Naidu, S.C.; Prathap, C.; Tripathu, J.; Singh, J.; Haque, S.M.; Rao, K.D.; Sahoo, N.K. Investigation on optical properties of spin coated TiO₂/Co composite thin films. *AIP Conf. Proc.* **2017**, *1832*, 080038. [[CrossRef](#)]
55. Adewinbi, S.A.; Buremoh, W.; Owwoeye, V.A.; Ajayeoba, Y.A.; Salau, A.O.; Busari, H.K.; Tijani, M.A.; Taleatu, B.A. Preparation and characterization of TiO₂ thin film electrode for optoelectronic and energy storage potentials: Effects of Co incorporation. *Chem. Phys. Lett.* **2021**, *779*, 138854. [[CrossRef](#)]
56. Islam, M.N.; Podder, J. The role of Al and Co co-doping on the band gap tuning of TiO₂ thin films for applications in photovoltaic and optoelectronic devices. *Mater. Sci. Semicond. Process.* **2021**, *121*, 105419. [[CrossRef](#)]

57. Boutlala, A.; Bourfaa, F.; Mahtili, M.; Bouaballou, A. Deposition of Co-doped TiO₂ thin films by sol-gel method. *IOP Conf. Ser. Mater. Sci. Eng.* **2016**, *108*, 012048. [[CrossRef](#)]
58. Waseda, Y.; Matsubara, E.; Shinoda, K. *X-ray Diffraction Crystallography: Introduction, Examples and Solved Problems*; Springer: Berlin/Heidelberg, Germany, 2011; ISBN 978-3-642-16634-1. [[CrossRef](#)]
59. Jauch, W.; Reehuls, M.; Bleif, H.J.; Kubanek, F.; Pattison, P. Crystallographic symmetry and magnetic structure of CoO. *Phys. Rev. B* **2001**, *64*, 052102. [[CrossRef](#)]
60. Wdowik, U.D.; Parlinski, K. Lattice dynamics of CoO from first principles. *Phys. Rev. B* **2007**, *75*, 104306. [[CrossRef](#)]
61. Moulder, J.F.; Stickle, W.F.; Sobol, P.E.; Bomben, K.D. *Handbook of X-ray Photoelectron Spectroscopy*; Physical Electronics, Inc.: Eden Prairie, MN, USA, 1995.
62. Crist, B.V. *Handbooks of Monochromatic XPS Spectra: Volume 1—The Elements and Native Oxides*; XPS International, Inc.: Ames, IA, USA, 1999.
63. Cole, K.M.; Kirk, D.; Thorpe, S. Co₃O₄ nanoparticles characterized by XPS and UPS. *Surf. Sci. Spectr.* **2021**, *28*, 014001. [[CrossRef](#)]
64. Velhal, N.B.; Yun, T.H.; Ahn, J.; Kim, T.; Kim, J.; Yim, C. Tailoring cobalt oxide nanostructures for stable and high-performance energy storage applications. *Ceram. Int.* **2023**, *49*, 4889–4897. [[CrossRef](#)]
65. Gong, B.; Luo, X.; Bao, N.; Ding, J.; Li, S.; Yi, J. XPS study of cobalt TiO₂ films prepared by pulsed laser deposition. *Surf. Interface Anal.* **2014**, *46*, 1043–1046. [[CrossRef](#)]
66. Naseem, S.; Pinchuk, I.V.; Luo, Y.K.; Kawakami, R.K.; Khan, S.; Husain, S.; Khan, W. Epitaxial growth of cobalt doped TiO₂ thin films on LaAlO₃(100) substrate by molecular beam epitaxy and their opto-magnetic based applications. *Appl. Surf. Sci.* **2019**, *493*, 691–702. [[CrossRef](#)]
67. Kim, J.; Livonen, T.; Hamalainen, J.; Kemell, M.; Meinander, K.; Mizohata, K.; Wang, L.; Raisanen, J.; Beranek, R.; Leskela, M.; et al. Low-temperature atomic layer deposition of cobalt oxide as effective catalyst for photoelectrochemical water-splitting devices. *Chem. Mater.* **2017**, *29*, 5796–5805. [[CrossRef](#)]
68. Biesinger, M.C.; Payne, B.P.; Grosvenor, A.P.; Lau, L.W.M.; Gerson, A.R.; Smart, R.S.C. Resolving surface chemical states in XPS analysis of first row transition metals, oxides and hydroxides: Cr, Mn, Fe, Co and Ni. *Appl. Surf. Sci.* **2011**, *257*, 2717–2730. [[CrossRef](#)]
69. Liu, T.; Guo, Y.F.; Yan, Y.M.; Wang, F.; Deng, C.; Rooney, D.; Sun, K.N. CoO nanoparticles embedded in the tree-dimensional nitrogen/sulfur co-doped carbon nanofiber networks as a bifunctional catalyst for oxygen reduction/evolution reactions. *Carbon* **2016**, *106*, 84–92. [[CrossRef](#)]
70. Li, X.C.; She, F.S.; Shen, D.; Liu, C.P.; Chen, L.H.; Li, Y.; Deng, Z.; Chen, Z.H.; Wang, H.E. Coherent nanoscale cobalt/cobalt oxide heterostructures embedded in porous carbon for the oxygen reduction reaction. *R. Soc. Chem.* **2018**, *8*, 28625. [[CrossRef](#)] [[PubMed](#)]
71. Chuang, T.J.; Brundle, C.R.; Rice, D.W. Interpretation of the X-ray photoemission spectra of cobalt oxides and cobalt oxide surfaces. *Surf. Sci.* **1976**, *59*, 413–429. [[CrossRef](#)]

Disclaimer/Publisher's Note: The statements, opinions and data contained in all publications are solely those of the individual author(s) and contributor(s) and not of MDPI and/or the editor(s). MDPI and/or the editor(s) disclaim responsibility for any injury to people or property resulting from any ideas, methods, instructions or products referred to in the content.